# SIMULTANEOUS ADSORPTION OF ANIONIC AND CATIONIC SPECIES ON UiO-66 AND MIL-125 MOFs: MECHANISMS & SELECTIVITY

Hugo G. Palhares, Pedro Andrade, Alain Moissette, Christophe Volkringer, Thierry Loiseau, Manuel Houmard, Eduardo H.M. Nunes

▶ **To cite this version:**

Hugo G. Palhares, Pedro Andrade, Alain Moissette, Christophe Volkringer, Thierry Loiseau, et al.. SIMULTANEOUS ADSORPTION OF ANIONIC AND CATIONIC SPECIES ON UiO-66 AND MIL-125 MOFs: MECHANISMS & SELECTIVITY. Microporous and Mesoporous Materials, 2024, Microporous and Mesoporous Materials, pp.113010. 10.1016/j.micromeso.2024.113010 . hal-04427892

**HAL Id: hal-04427892**
**https://hal.univ-lille.fr/hal-04427892**

Submitted on 12 Feb 2024

**HAL** is a multi-disciplinary open access archive for the deposit and dissemination of scientific research documents, whether they are published or not. The documents may come from teaching and research institutions in France or abroad, or from public or private research centers.

L'archive ouverte pluridisciplinaire **HAL**, est destinée au dépôt et à la diffusion de documents scientifiques de niveau recherche, publiés ou non, émanant des établissements d'enseignement et de recherche français ou étrangers, des laboratoires publics ou privés.

# SIMULTANEOUS ADSORPTION OF ANIONIC AND CATIONIC SPECIES ON UiO-66 AND MIL-125 MOFs: MECHANISMS & SELECTIVITY

Hugo G. Palhares[1,*], Pedro H. M. Andrade[2], Alain Moissette[2], Christophe Volkringer[3], Thierry Loiseau[3], Manuel Houmard[4,5], Eduardo H.M. Nunes[1,5,⊗]

(1) Departamento de Engenharia Metalúrgica e de Materiais (DEMET), Universidade Federal de Minas Gerais (UFMG), CEP: 31270-901, Belo Horizonte, Brazil.

(2) Laboratoire de Spectroscopie pour les Interactions, la Réactivité et l'Environnement (LASIRE), Université de Lille – Sciences et Technologies, 59655 - Villeneuve d'Ascq, France.

(3) Unité de Catalyse et Chimie du Solide (UCCS), Univ. Lille, CNRS, Centrale Lille, Univ. Artois, UMR 8181 - UCCS, F-59000 Lille, France

(4) Departamento de Engenharia Química, Universidade Federal de Minas Gerais, Pampulha, CEP: 31270-901, Belo Horizonte, MG, Brasil.

(5) Centro de Tecnologia em Nanomateriais e Grafeno (CTNano), Rua Professor José Vieira de Mendonça, 520 – Engenho Nogueira, Belo Horizonte – MG, CEP: 31310-260, Brasil.

***** hgpalhares@ufmg.br

⊗ eduardo.nunes@demet.ufmg.br

# ABSTRACT

Metal-organic frameworks (MOFs) have attractive properties, including regular pore structure, high specific surface area, tunable surface properties, and abundant active sites. Such properties have boosted their recent development in many fields, including water treatment. In this study, MOFs composed of tetravalent metals ($Ti^{4+}$ and $Zr^{4+}$) and dicarboxylate linker (terephthalate – BDC) were modified using surface functionalization and/or pore structure through defect engineering to enhance adsorption properties. It has been shown that the Ti-containing materials (MIL-125) show a greater affinity for cationic species, while the Zr-containing samples (UiO-66) have a higher affinity for anionic species. Surface charge and electrostatic interactions could account for such a difference in adsorption properties. Zeta potential measurements showed that MIL-125 has a more negative surface charge for both non-functionalized and amino-functionalized versions, which favors the interaction with cationic molecules. On the other hand, UiO-66 has a more positive surface, which facilitates interactions with anionic molecules. Within each MOF family, the non-functionalized structures emerged as the best-performing materials. Specifically, MIL-125(H) and UiO-66(H)_5eq, with 5eq denoting the amount of $H_2O$ added during synthesis, showed superior performance. Furthermore, by performing simultaneous adsorption experiments with anionic and cationic contaminants, it was found that the adsorption of the anionic dye acid orange 7 (AO7) onto the UiO-66 framework is primarily based on specific interactions between the sulfonic group ($-SO_3^-$) within the AO7 molecule and the inorganic core $Zr_6O_4(OH)_4$ of UiO-66. The interaction between MIL-125 and the cationic dye methylene blue (MB) was found to be more delocalized, based on electrostatic and π-π interactions between the benzene domains. Finally, except for MIL-125(H), all the tested MOFs showed high stability in water and in the adsorption process. The higher stability of UiO-66 over MIL-

125 materials can be attributed to steric effects and lower metal electronegativity. Compared to MIL-125(H), the higher stability of MIL-125($NH_2$) is probably related to the formation of intramolecular hydrogen bonds.

## Keywords

Metal-organic frameworks; UiO-66; MIL-125; organic dyes; simultaneous adsorption.

## 1. Introduction

Metal–Organic Frameworks (MOFs) have recently emerged as novel materials for applications in many fields, including water purification [1–3]. The remarkable properties of these materials, such as their pronounced porosity resulting from a well-defined intrinsic pore structure and the abundance of active sites, have driven their recent and substantial progress [1,4–6]. Among the many options for the preparation of such materials, the use of tetravalent metal MOFs such as MIL-125 and UiO-66 has been of particular interest in many studies. Their typical robustness in harsh environments and relatively high permanent porosity are often cited as reasons for this preference [7,8]. Their usual stability can be explained by the strong coordination bonds between the hard Lewis acid (tetravalent metal) and the hard Lewis base (carboxylate moieties) that form their framework. Furthermore, their structural rigidity and high coordination number also help to protect such materials from chemical attack by guest molecules [9–11]. Such properties make them suitable candidates for water treatment, as many MOFs exhibit poor stability in humid environments [12]. Although UiO-66 has systematically shown high stability in water [13,14], some studies have reported that MIL-125 has some instability [15,16].

In a recent work [17], we modified the crystalline structure of UiO-66(H) (where 'H' indicates the use of the terephthalate – BDC – linker) by using different additives and adjusting the synthesis conditions. The primary objective of this study was to achieve precise control of defects within the MOF framework, resulting in improved adsorption capabilities for anionic compounds at the expense of their cationic counterparts. The synthesis of its aminated version UiO-66($NH_2$) (where '$NH_2$' indicates the use of the 2-aminoterephthalate linker) was now studied using different amounts of $H_2O$, in low molar ratios, which was observed to give the best results both in morphology control and adsorption performance. Thus, the different versions, functionalized ($NH_2$) and non-functionalized (H), could be compared in terms of their structure, surface properties, and adsorption behavior. In addition, we also investigated the adsorption of other tetravalent MOFs, MIL-125(H) and MIL-125($NH_2$), due to their well-known stability. Furthermore, these structures are expected to have a more negative surface charge compared to UiO-66, which can greatly influence the adsorption mechanism of various positively charged pollutants [17,18]. The crystalline structure of MIL-125 could not be obtained when water was used in the synthesis step. Thus, the synthesis described here was based on the standard synthesis developed in another work [19]. The aim of this study is a comparative evaluation of the structural features and stability of two closely related MOFs ($M^{4+}$-BDC) with different crystal frameworks, pore structures, and surface properties. Furthermore, the effect of these differences on the adsorption behavior of anionic and cationic molecules will be investigated, while also attempting to elucidate the different adsorption mechanisms involved in the application of different adsorption systems.

# 2. Materials and Methods

## 2.1. Synthesis

### - UiO-66

The synthesis followed a procedure similar to that described in a previous work [17]. Briefly, 8 mmol of zirconium tetrachloride ($ZrCl_4$, Sigma Aldrich, 99.5%) and 8 mmol of either 1,4-benzenedicarboxylic acid ($H_2BDC$, Sigma Aldrich, 98%) or 2-aminoterephthalic acid ($H_2BDC(NH_2)$, Sigma Aldrich, 99%) were initially mixed with 40 mL of N,N-dimethylformamide (DMF, Sigma-Aldrich, 99.8 %). Subsequently, 40 mL of DMF solution containing X molar equivalents of $H_2O$ relative to $ZrCl_4$ was slowly added to the previously prepared solution. The samples prepared without the addition of water were obtained using a less concentrated synthesis, employing 1.6 mmol of precursors instead of 8 mmol. For a more detailed description of this approach, please refer to our previous work [17]. The resulting solution was poured into a Teflon-lined stainless steel autoclave and kept under autogenous pressure at 120 °C for 24 h. After cooling to room temperature, the resulting crystalline powder was washed twice with DMF and absolute ethanol (EtOH, Synth, 99.5%), using 20 ml for each washing step. The obtained precipitate was then sonicated in EtOH (50 mL) for 30 min, dried, and then activated in air at 100 °C. The samples were designated as UiO-66(H)_Xeq or UiO-66($NH_2$)_Xeq, where X represents the amount of water added to the synthesis. UiO-66(H) and UiO-66 ($NH_2$) refer to non-modified and amino-functionalized samples, respectively.

### - MIL-125

MIL-125(H) was prepared by a solvothermal route as described in detail in a previous work[19]. A solution containing 4.5 mL of DMF (Sigma Aldrich, 99.8% anhydrous) and 0.5 mL of methanol (MeOH, Sigma Aldrich, 99.8% anhydrous) was initially prepared under Ar atmosphere inside a glove box (JACOMEX, GP Campus model). Then, 300 µL of titanium tetraisopropoxide (TTIP, Sigma Aldrich, 97%) and 459 µL of butyric acid (Sigma Aldrich, ≥ 99%) were added to the previous solution and kept under stirring for 5 min. Then, 250 mg of $H_2BDC$ was added and kept under stirring for another 10 min. The resulting mixture was poured into a 25 mL stainless steel autoclave at 120 °C for 24 h. A white powder was recovered by centrifugation and washed three times with DMF and MeOH, with 20 ml in each washing step. Finally, it was calcined in air at 200 °C for 12 h.

MIL-125($NH_2$), an amino-modified sample, was prepared by a similar solvothermal route described for MIL-125(H) [19]. A solution containing 4.5 mL of DMF and 0.5 mL of MeOH was prepared under an Ar atmosphere inside a glove box. Subsequently, 300 µL of titanium tetraisopropoxide (TTIP, Sigma Aldrich, 97%) was added dropwise and stirred for 5 min. Then, 418 mg of $H_2BDC(NH_2)$ was added and kept under stirring for 10 min. Subsequently, 4 mL of MeOH was added to the mixture. The mixture was then placed in a 25 mL stainless steel autoclave at 150 °C for 16 h. A yellow powder was obtained by centrifugation and washed three times with DMF and MeOH, with 20 ml in each washing step. Finally, it was calcined in air at 100 °C for 12 h.

## 2.2. Characterizations

X-ray powder diffraction (XRD) was conducted on a PANalytical Empyrean diffractometer at a scan rate of $0.03°.s^{-1}$, using $CuK_\alpha$ as the radiation source ($\lambda$ = 1.54 Å).

Transmission electron microscopy (TEM) was conducted on a Tecnai G2-12 - FEI SpiritBiotwin microscope at an accelerating voltage of 120 kV. The samples used in these tests were previously dispersed in EtOH and sonicated at room temperature for 5 min. The as-obtained suspensions were dripped on carbon-coated grids (Holey Carbon) and air-dried at room temperature. $N_2$ sorption tests were conducted at -196 °C on a BELSORP-max analyzer using samples outgassed under vacuum at 100 °C for 12 h. The specific surface area (SSA) was evaluated by the multipoint BET (Brunauer-Emmett-Teller) model following the consistency criteria [7,20]. The non-local density functional theory (NLDFT) and Barrett-Joyner-Halenda (BJH) method were employed to evaluate the pore size distribution of the examined materials. Thermogravimetry (TG) was performed on an Exstar 7200 thermal analyzer at a heating rate of 10 °C.min$^{-1}$ and under $N_2$ flow (20 mL.min$^{-1}$). Dynamic light scattering (DLS) and Zeta potential (ζ) were measured at room temperature using a ZetaPlus apparatus (Brookhaven Instruments). The particles were first dispersed in deionized water (concentration 0.10 mg.mL$^{-1}$) using an ultrasonic bath for 5 min. The pH of the solution was then adjusted to the desired value using aqueous solutions of HCl and NaOH (0.1 M). A minimum of 20 measurements were made for each suspension after redispersion. FTIR spectroscopy was performed using a Bruker Alpha spectrometer equipped with an attenuated total reflectance module. A diamond crystal was used as the reflecting element in these tests. Spectra were recorded from 4000 to 400 cm$^{-1}$ with a resolution of 4 cm$^{-1}$ and 128 scans.

### 2.3. Adsorption Tests

Batch adsorption tests were carried out at room temperature using aqueous solutions containing 20 mg.L$^{-1}$ of acid orange 7 (AO7 / Sigma-Aldrich) and/or methylene blue (MB / Synth). The molecular structure of these dyes in the ionic form is presented in the

Supplementary Material (Fig. S1). The adsorbent loading in these solutions was 100 $mg.L^{-1}$ unless otherwise specified. As will be discussed in more detail later, the motivation for this approach stems from the significantly greater adsorption capacity of MIL-125 compared to UiO-66. Consequently, to perform a more meaningful kinetic study for both samples while keeping the dye concentration consistent in all tests (20 $mg.L^{-1}$), it became imperative to change the initial concentration of MIL-125 from 100 $mg.L^{-1}$ to 50 $mg.L^{-1}$. The initial pH of these aqueous solutions was about 5 and remained nearly constant during the adsorption tests. Aliquots collected during the test were centrifuged at 3000 rpm for 10 min. The particle-free supernatant was then transferred to quartz cuvettes and examined by Ultraviolet-Visible (UV-Vis) spectroscopy on a Shimadzu UV-2600 spectrometer with a resolution of 1 nm. The light absorption at 484 nm and 664 nm were used as references for AO7 and MB, respectively. The removal efficiency (R – %) was determined from Eq. (1), where $C_e$ represents the concentration at equilibrium ($t = t_e$).

$$R = \left(\frac{C_0 - C_e}{C_0}\right) \times 100 \quad (1)$$

Kinetic calculations were performed based on the integrated form of the pseudo-second-order kinetic model (Eq. 2), where $k_2$ represents the rate constant ($g.mg^{-1}.min^{-1}$), $q_e$ is the adsorption capacity at equilibrium ($mg.g^{-1}$), and $q_t$ is the adsorption ($mg.g^{-1}$) measured at time t (min). Adsorption systems similar to those studied in this work have been described using this model [17,21–24].

$$q_t = \frac{k_2 q_e^2 t}{1 + k_2 q_e t} \quad (2)$$

# 3. Results and Discussion

## 3.1. Characterization results

Figure 1 shows the XRD patterns obtained for the samples prepared in this study. The incorporation of amino groups into the parent materials UiO-66(H) and MIL-125(H) did not cause any substantial changes in their crystal structures, as supported by the constancy of the Bragg diffraction peaks at their original positions. The UiO-66 samples showed broadened diffraction peaks for $H_2O$ additions above 10 eq., indicating a reduction in crystallinity due to the presence of framework defects in these samples. For smaller amounts of $H_2O$, the crystal size remains approximately the same, mainly in the range of 100-300 nm (Figure 2b,d). However, the crystals lose their typical octahedral morphology, which is only observed for water-free samples (Figure 2a,c). This was also observed in our previous work [17]. MIL-125(H) and MIL-125($NH_2$) showed a morphological mixture of irregular plates and crystals with the typical decahedral or truncated square pyramidal (Figure 2e,f) [18,25], which have been identified with dashed blue circles. MIL-125(H) has crystals in a wider size range than MIL-125($NH_2$), as the former has crystals in the range of 100-300 nm, while the latter has crystals in a narrower range of about 100 nm. This difference can be due to the increased solubility of $NH_2$-BDC in DMF, which accelerates the kinetics of framework formation compared to H-BDC.

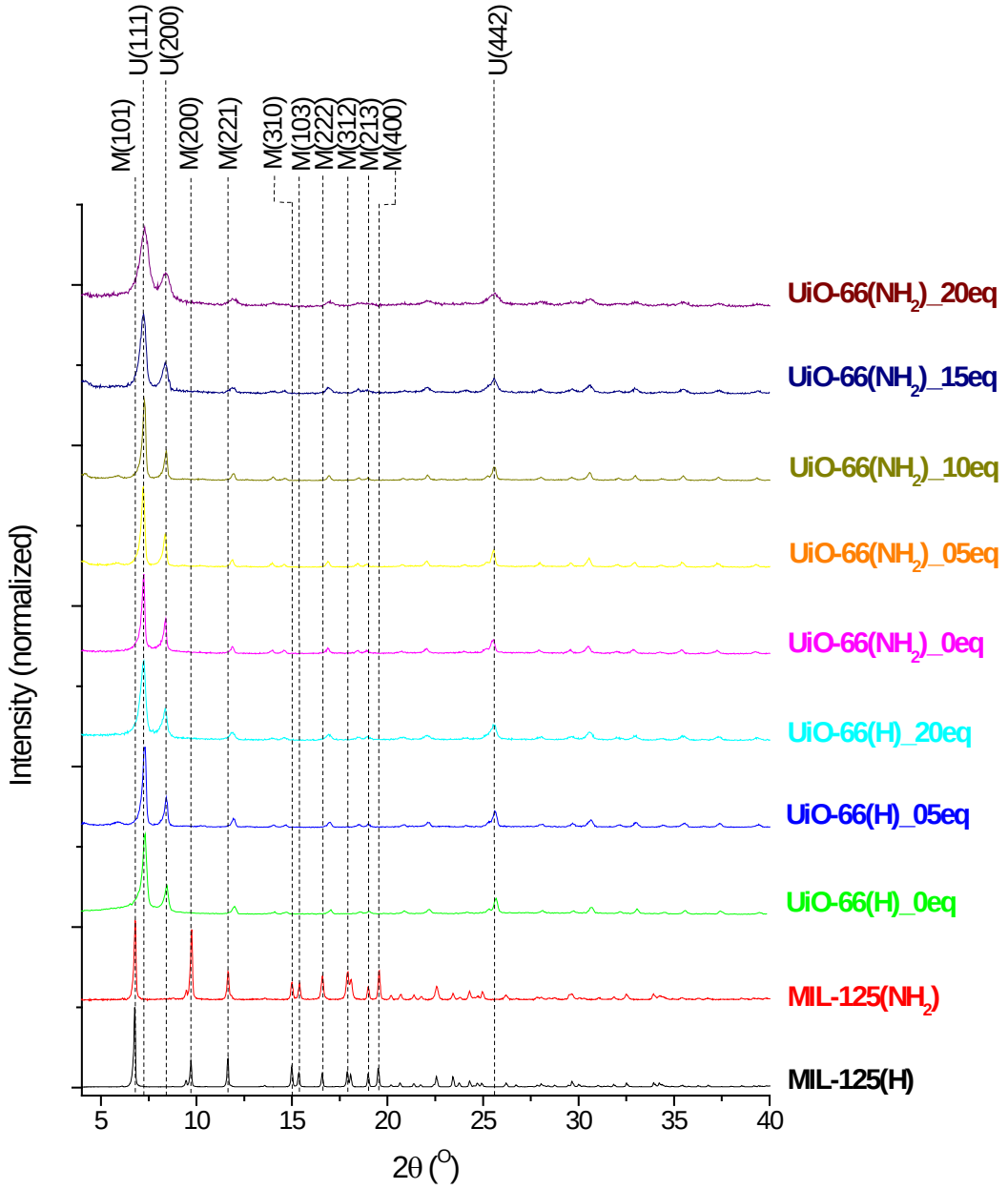


*Figure 1: XRD patterns of the synthesized MOFs; UiO-66 and MIL-125, with and without functionalization with amino groups (-$NH_2$). Different UiO-66 samples were obtained by varying the amount of $H_2O$ (in molar equivalents). The main diffraction peaks were indexed according to other works* [26,27].

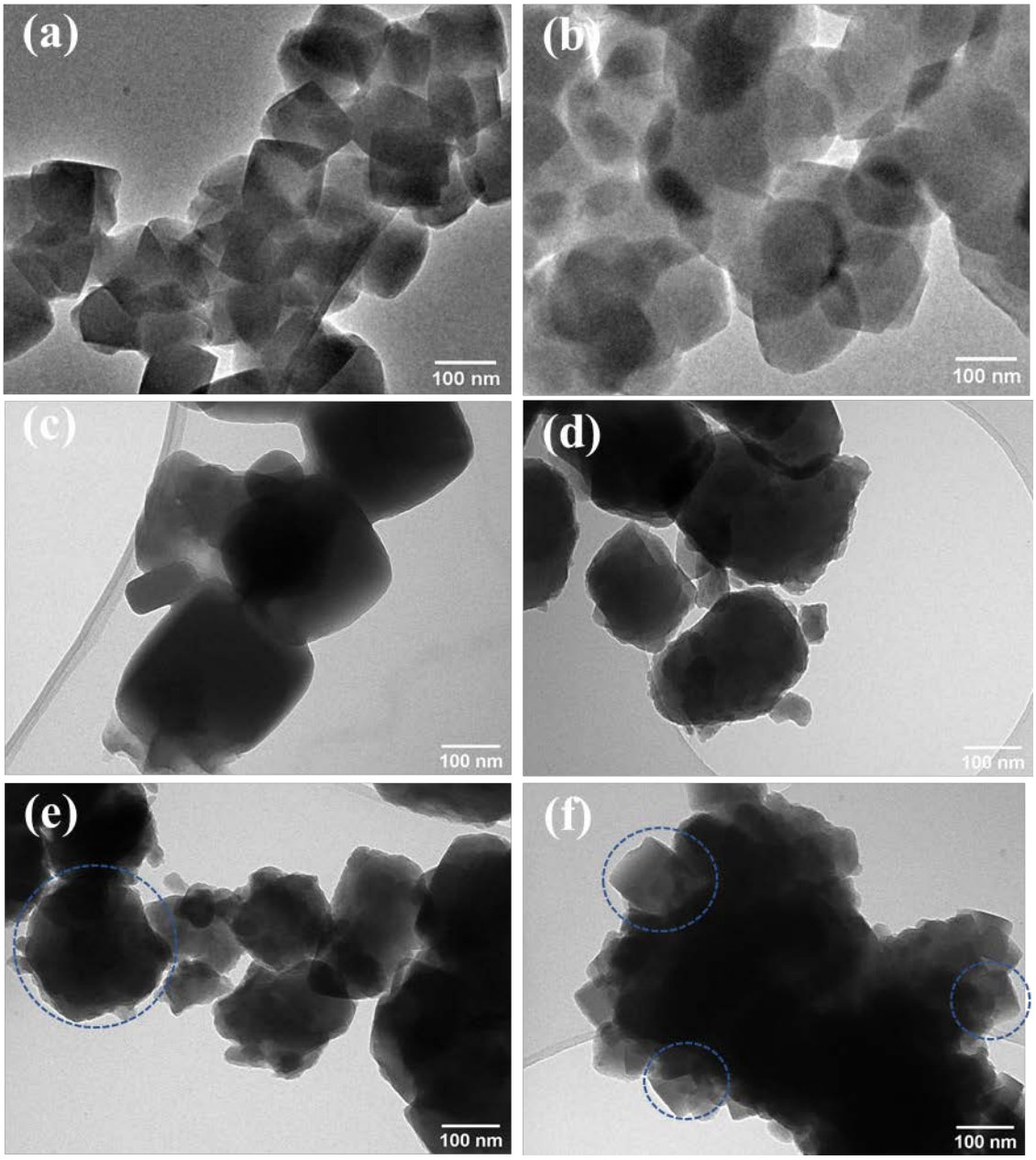


*Figure 2: TEM micrographs of UiO-66(H)_0eq (a), UiO-66(H)_5eq (b), UiO-66($NH_2$)_0eq (c), UiO-66($NH_2$)_10eq (d), MIL-125(H) (e) and MIL-125($NH_2$) (f). The scale bars represent 100 nm and the dashed blue circles highlight the typical decahedral or truncated square pyramidal structure of these MOFs.*

Figure 3 shows the $N_2$ sorption isotherms collected and pore size distributions obtained using the NLDFT and BJH models. Typically, MIL-125 has micropores that consist of tetrahedral and octahedral cages, with diameters of about 6.1 and 12.5 Å, respectively

[28]. The microporous structure of UiO-66 is also formed by cages of similar morphology but with diameters of 9 and 11 Å [29]. The prepared samples generally show negligible mesoporosity and high microporosity, as evidenced by the absence of a hysteresis loop in the isotherms obtained. The only sample that showed a degree of mesoporosity was obtained using a greater quantity of $H_2O$ in the synthesis (i.e., 20 eq.), following the same trend as the previous study for the non-amined version of UiO-66 [17]. However, there is a significant discrepancy in the microporous structure of the different UiO-66($NH_2$)_Xeq samples obtained here. We already showed in another work that the addition of $H_2O$ induces an expansion of the microporous network of UiO-66(H) in both the tetrahedral and octahedral cages, leading to the formation of defects in the MOF structure [17]. As shown in Figure 3-c, the use of $H_2O$ in the synthesis of UiO-66($NH_2$) resulted in a decrease in the tetrahedral pores and an increase in the octahedral pores. At first glance, this observation seems to contradict the previous hypothesis, since an increase in both pores should be observed. However, it can be inferred that the reduction of such pores is associated with the growth of different crystals, producing particles of interconnected crystals. This phenomenon is commonly observed for MOFs due to their intrinsic porosity, especially in syntheses carried out in more concentrated reaction media such as those used in this study [30,31]. This behavior is consistent with the micrographs obtained, which show crystals with irregular shapes typical of the interpenetration of multiple crystals. This phenomenon is schematized in Figure 4. For comparison purposes, the pore distribution of UiO-66(H)_5eq, the sample that showed the highest pore expansion, has also been included. It can be observed that this material has tetrahedral pores similar to those of UiO-66($NH_2$)_0eq (about 1.0-1.1 nm) but with larger octahedral pores (1.8 vs. 1.6 nm).

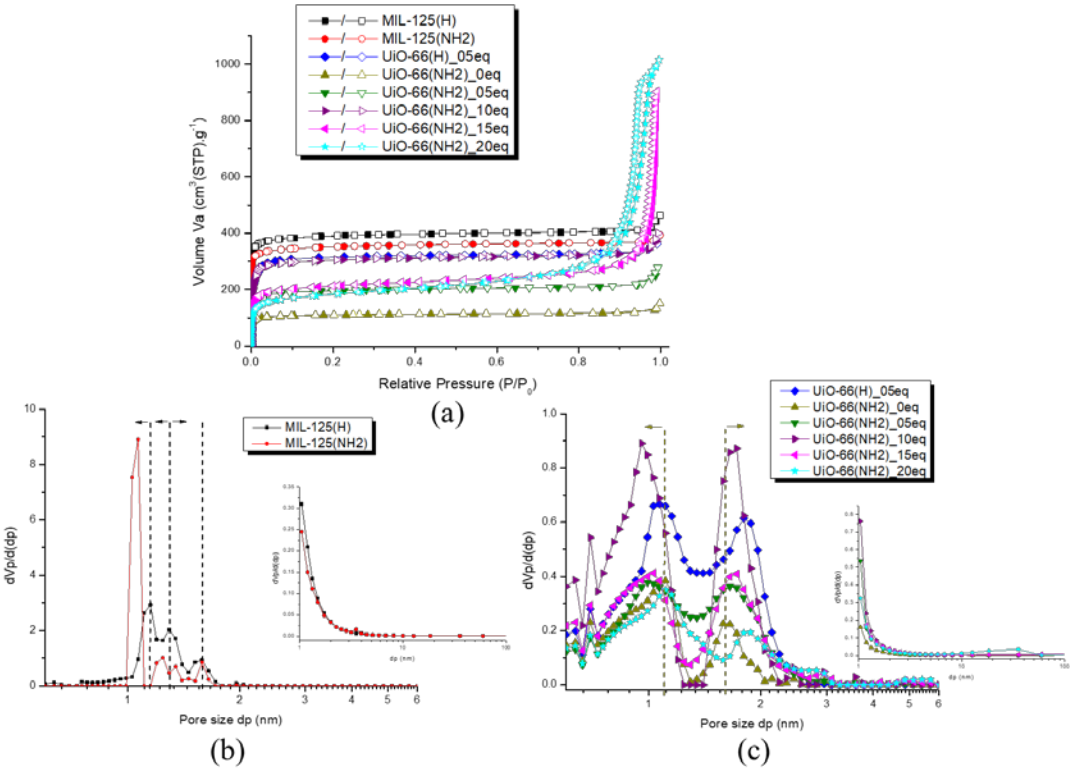


*Figure 3: (a) $N_2$ sorption isotherms and pore size distributions evaluated for (b) MIL-125(X) and (c) UiO-66(X)_Y. The closed and open symbols present in the isotherms refer to the adsorption and desorption branches, respectively.*

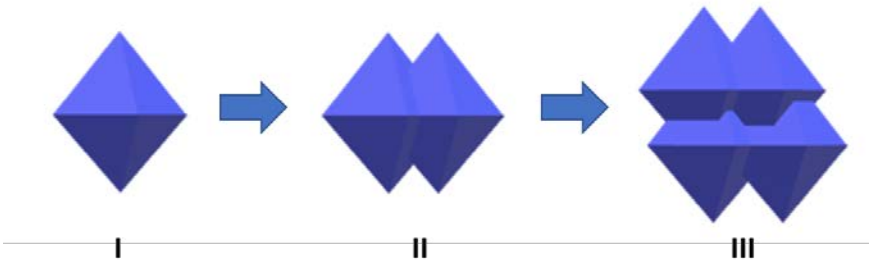


*Figure 4: Schematic representation of the effect of concatenated growth of different MOF crystals: I) representation of a single crystal; II) interpenetration of 2 crystals and III) interpenetration of multiple crystals.*

Table 1 summarizes the textural characteristics obtained from the $N_2$ sorption tests. It can be inferred that the specific surface areas of MIL-125 are higher than those of UiO-66. This behavior is in agreement with the theoretical and experimental values found in the literature [14,28]. It should also be noted that the aminated versions of these materials have slightly lower porosity and SSA. A partial blocking of the MOF pores by the $NH_2$ groups may be responsible for this behavior. It can also be observed that despite a slight decrease in the size of the tetrahedral pores, as discussed previously, there was still a significant increase in porosity and SSA with the addition of $H_2O$ in the synthesis of UiO-66($NH_2$)_X, reaching a maximum value at X = 10 eq. ($V_{micro}$ = 0.46 $cm^3.g^{-1}$ and SSA = 1240 $m^2.g^{-1}$). Nevertheless, we observed a decrease in porosity and SSA for higher water contents (*e.g.* $V_{micro}$ = 0.27 $cm^3.g^{-1}$ and SSA = 679 $m^2.g^{-1}$ for X = 20 eq.). Thus, even though the concatenation of the crystals tends to decrease these properties, the introduction of defects due to the presence of $H_2O$ can compensate for and even overcome this effect, producing structures with higher porosity and SSA. It has already been shown that such defects are mainly composed of missing linkers [17], which also occur in synthesis using HCl as an additive [32]. In both cases, chlorine and hydroxyl groups would compensate for the missing linkers [17,33].

*Table 1: Textural properties evaluated from the $N_2$ sorption isotherms. $V_{total}$ was measured at $P/P_0 = 0.91$, corresponding to pores of up to 20 nm.*

| Sample | SSA ($m^2.g^{-1}$) | $V_{micro}$ ($cm^3.g^{-1}$) | $V_{meso}$ ($cm^3.g^{-1}$) | $V_{total}$ ($cm^3.g^{-1}$) |
|---|---|---|---|---|
| MIL-125(H) | 1569 | 0.59 | 0.04 | 0.63 |
| MIL-125($NH_2$) | 1411 | 0.53 | 0.04 | 0.57 |
| UiO-66(H)_5eq | 1280 | 0.48 | 0.04 | 0.52 |
| UiO-66($NH_2$)_0eq | 437 | 0.17 | 0.02 | 0.19 |
| UiO-66($NH_2$)_5eq | 797 | 0.29 | 0.04 | 0.33 |
| UiO-66($NH_2$)_10eq | 1240 | 0.46 | 0.05 | 0.51 |
| UiO-66($NH_2$)_15eq | 831 | 0.35 | 0.11 | 0.46 |
| UiO-66($NH_2$)_20eq | 679 | 0.27 | 0.34 | 0.61 |

The samples were also examined in terms of surface charge using Zeta potential measurements (Figure 5). In general, UiO-66 samples showed a higher point of zero charge (PZC) than MIL-125 samples, except for UiO-66($NH_2$)_15eq. These values are consistent with those found in the literature, with values close to 6 for UiO-66 and below 5 for MIL-125 [18,34,35]. However, it can be observed that the addition of $H_2O$ in the synthesis of UiO-66($NH_2$) generated particles with a more negative charge, shifting the Zeta potential curve toward a lower pH and decreasing the PZC value. The maximum shift is observed in the sample with 15 eq. of $H_2O$. The PZC value of UiO-66($NH_2$)_10eq and UiO-66($NH_2$)_20eq decreased to about 5.5, while the PZC of UiO-66($NH_2$)_15eq decreased to a value close to 4.5. This behavior was not observed for UiO-66(H), whose PZC remained stable around 6. TG tests were also performed (Supplementary Material – Fig. S2) and the samples displayed similar behavior compared to other studies [17,28,36–40]. Typically, the aminated version of UiO-66 has lower thermal stability compared to

its original non-aminated counterpart. On the other hand, UiO-66(H) exhibited a complete collapse of the framework at temperatures slightly higher than those observed for MIL-125 (560 ºC vs. 500 ºC).

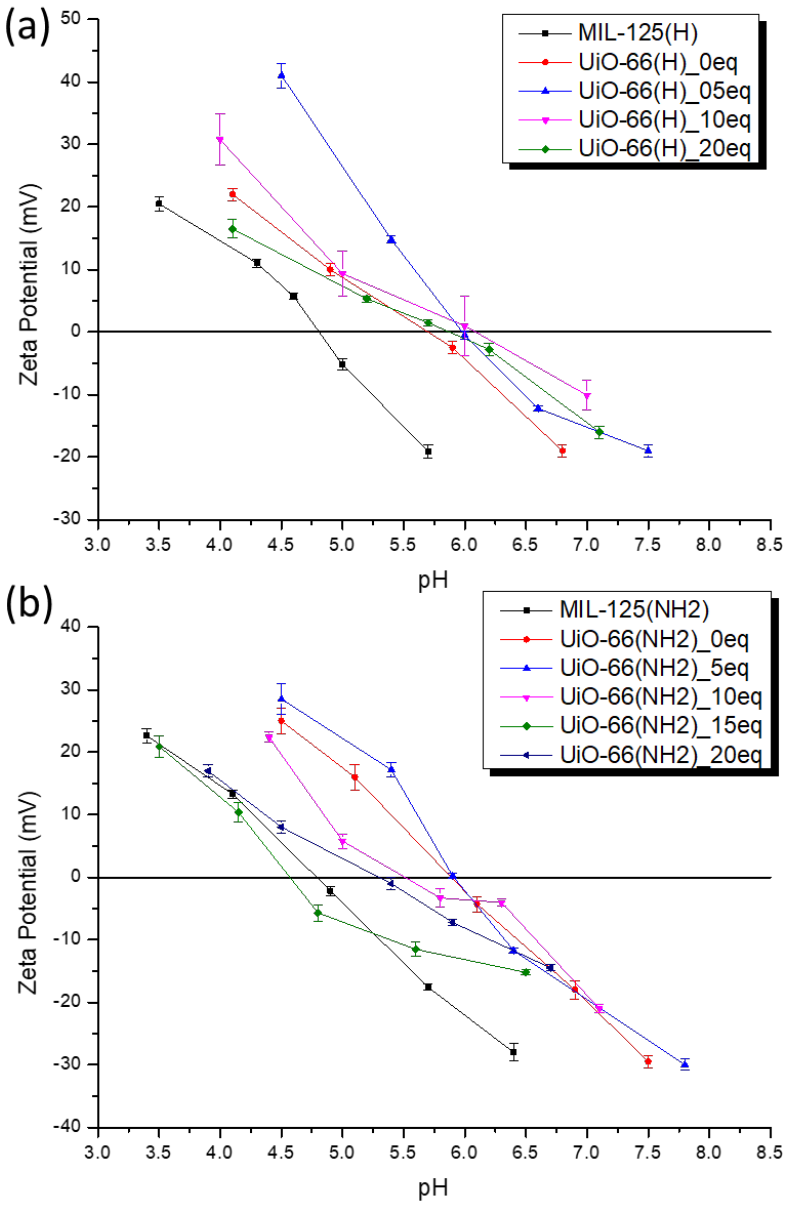


*Figure 5: Zeta potential ζ measurements of MIL-125 and UiO-66 samples, without (a) and with (b) functionalization with amino groups (-$NH_2$).*

### 3.2. Adsorption of anionic and cationic species from single solutions

The adsorption of different dyes, namely anionic AO7 and cationic MB, was initially studied using solutions containing only one of the contaminants (single solutions of either AO7 or MB). These oppositely charged molecules were selected due to their similar dimensions (1.57×1.00×0.54 nm for AO7 and 1.63×0.79×0.40 nm for MB) – Fig. S1 (Supplementary Material). MB is slightly smaller than AO7, which allows for a meaningful comparison of adsorption based on the inherent electrostatic nature of these molecules. In addition, these dimensions match the pore size measured by $N_2$ sorption (Figure 3). The influence of adding $H_2O$ during the synthesis of UiO-66($NH_2$) was thus compared with the optimized sample obtained in a previous study [17], here referred to as UiO-66(H)_5eq. For a more thorough comparison, UiO-66(H)_0eq and UiO-66(H)_20eq were also included. The adsorption curves obtained from solutions containing 20 ppm of AO7 or MB are shown in the supplementary material (Fig. S3). Summarized data, along with results obtained using the pseudo-second-order kinetics model, are presented in Table 2. Note that because the initial concentration (100 $mg.L^{-1}$) was found to be excessive, the adsorption performance of MIL-125 for the cationic dye MB is presented for two concentrations of MOF (50 and 100 $mg.L^{-1}$). In general, it can be seen that the MIL-125 samples have a higher affinity for the cationic pollutant MB, whereas the UiO-66 materials have a stronger affinity for the anionic dye AO7, as indicated by the calculated adsorption capacities ($q_e$) presented in Table 2. However, an opposite trend was observed when the water volume was increased during the synthesis of UiO-66($NH_2$). The adsorption behavior of the different materials (Table 2) can be strongly correlated with their surface charge (based on Figure 5) and textural properties (Figure 3 and Table 1). Higher SSA and larger pores are associated with faster adsorption

kinetics and higher adsorption capacities. At the same time, the surface charge plays a critical role in determining the preference for adsorption of either positively or negatively charged pollutants. Among the UiO-like samples, UiO-66(H)_5eq showed superior adsorption efficiency for capturing AO7 molecules, while among the MIL-like samples, MIL-125(H) emerged as the most effective material for adsorbing MB molecules. The non-aminated versions of each MOF family performed better than the aminated versions in both cases.

The presence of amino groups in the structure of MOFs has been associated with their greater electronegativity and affinity for cationic molecules such as MB. This is due to the ability of the amino group to form hydrogen bonds with the cationic molecules, as well as the availability of an electron pair on the nitrogen atom [15,18]. Because of that, it was observed higher adsorption of MB on the functionalized versions of MIL-125. However, this behavior was not reproduced with the samples synthesized in this study, most likely due to the lower porosity (and SSA) and the presence of typically smaller pores in MIL-125($NH_2$) compared to MIL-125(H) (Figure 3b). Since the pore dimensions are close to the molecular size of MB, the slightly larger pore distribution of MIL-125(H) undoubtedly contributes to improved accessibility and interaction of MB on the MOF surface.

Concerning the UiO-66 samples, a greater affinity of MB was observed for the aminated versions, mainly with the decrease in the PZC value in the samples synthesized with greater amounts of water (from 5.9 to 4.6), as previously discussed. This relationship is exhibited in Figure 6, where the difference in affinity for anionic and cationic groups is clear. In addition to the amino groups acting as a specific MB adsorption site, it also

favors electrostatic interaction, making the surface more negatively charged in syntheses with greater additions of water. This behavior enhances the adsorption of cationic species. Furthermore, the broader and typical bimodal pore size distribution observed for UiO-66 compared to MIL-125, with some pores over 2 nm (Figure 3), allows easy access throughout the porous structure for both MB and AO7. This feature is particularly advantageous for AO7 due to its slightly larger molecular size.

The non-aminated version of UiO-66 shows a minimum MB adsorption at 5 eq. of $H_2O$, which coincides with a maximum for AO7 adsorption. These observations are consistent with the values of Zeta potential measured for these samples, which is much more positive for UiO-66(H)_5eq compared to the other samples. Its higher SSA and more positive surface charge explain its greater tendency to interact with anionic species and repel cationic ones, contributing to its greater affinity for anionic species. Regarding the functionalized UiO-66($NH_2$) samples, the one with the best selectivity was UiO-66($NH_2$)_10eq, with a removal efficiency ratio AO7/MB of 2.2. However, this value is still well below the optimal selectivity determined in single solution tests using UiO-66(H)_5eq, with the high removal efficiency ratio AO7/MB of 10.7. Such samples, together with MIL-125 were then compared in adsorption tests performed using a mixture of AO7 and MB. The adsorption process in solutions containing both dyes can be evaluated in these tests.

*Table 2: Summary of the adsorption kinetics of AO7 and MB for both MIL-125 and UiO-66-like structures, with the removal efficiency measured at 180 min. Unless otherwise specified, the MOF concentration used was 100 mg.L$^{-1}$. The best-performing material for each contaminant is highlighted.*

| **Adsorbent** | **Pollutant** | **$k_2 \times 10^{-3}$ (g.mg$^{-1}$.min$^{-1}$)** | **$q_e$ (mg.g$^{-1}$)** | **$R^2$** | **Removal Efficiency (%)** |
|---|---|---|---|---|---|
| MIL-125(H) | AO7 | 0.18 | 27.1 | 0.76 | 5 |
| **MIL-125(H)** | **MB** | **3.54** | **202.8** | **0.999** | **100** |
| **MIL-125(H)_50mg.L$^{-1}$** | **MB** | **0.09** | **417.0** | **0.986** | **95** |
| MIL-125(NH2) | AO7 | 0.09 | 41.6 | 0.915 | 8 |
| MIL-125(NH2) | MB | 0.77 | 204.9 | 0.999 | 99 |
| MIL-125(NH2)_50mg.L$^{-1}$ | MB | 0.59 | 238.9 | 0.986 | 61 |
| UiO-66(H)_0eq | AO7 | 0.56 | 68.3 | 0.944 | 43 |
| UiO-66(H)_0eq | MB | 1.37 | 39.5 | 0.974 | 19 |
| **UiO-66(H)_5eq** | **AO7** | **2.85** | **191.5** | **0.999** | **96** |
| UiO-66(H)_5eq | MB | 15.2 | 19.6 | 0.987 | 9 |
| UiO-66(H)_20eq | AO7 | 1.06 | 186.1 | 0.992 | 92 |
| UiO-66(H)_20eq | MB | 0.95 | 101.2 | 0.973 | 50 |
| UiO-66($NH_2$)_0eq | AO7 | 48.3 | 12.2 | 0.988 | 6 |
| UiO-66($NH_2$)_0eq | MB | 1.50 | 20.5 | 0.977 | 9 |
| UiO-66($NH_2$)_5eq | AO7 | 0.47 | 177.5 | 0.996 | 84 |
| UiO-66($NH_2$)_5eq | MB | 0.63 | 100.9 | 0.994 | 47 |
| UiO-66($NH_2$)_10eq | AO7 | 0.42 | 191.0 | 0.998 | 89 |
| UiO-66($NH_2$)_10eq | MB | 0.86 | 81.2 | 0.970 | 40 |
| UiO-66($NH_2$)_15eq | AO7 | 1.17 | 100.5 | 0.997 | 49 |
| UiO-66($NH_2$)_15eq | MB | 0.74 | 133.7 | 0.987 | 66 |
| UiO-66($NH_2$)_20eq | AO7 | 2.37 | 75.7 | 0.991 | 38 |
| UiO-66($NH_2$)_20eq | MB | 0.73 | 123.3 | 0.972 | 61 |

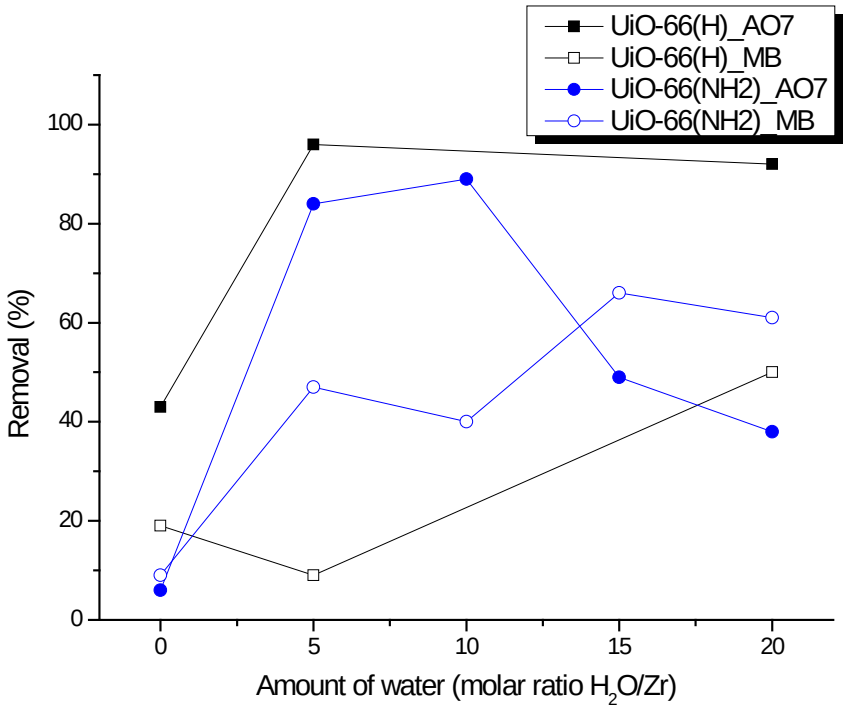


*Figure 6: AO7 and MB removal capacity of the different synthesized UiO-66 samples, with and without amino group, as a function of the different amounts of $H_2O$ used in the synthesis. The values refer to the end of the test (180 min) using 20 ppm of the dyes and 100 mg.L$^{-1}$ of the different materials.*

## 3.3. Simultaneous adsorption of anionic and cationic species – adsorption mechanisms

In this section, selected samples with the best adsorption properties from each class of synthesized MOFs were investigated by performing additional adsorption tests using a mixture of AO7 and MB at a concentration of 20 mg.L$^{-1}$ each. Figure 7 shows the absorbance spectra of various concentrations of the prepared mixtures compared to the spectra of the pure dyes. It can be observed that the mixture of these contaminants produces a moss-green colored solution whose absorption spectrum does not exactly match the sum of the spectra of the two contaminants when separated. This change is

more pronounced for MB in the spectral region between 550 and 700 nm. Although no references were found in the literature regarding the interaction of MB with other molecules similar to AO7, studies of the interaction between MB molecules themselves may help in understanding the possible mechanism associated with such an event [41,42]. From these studies, it can be realized that the MB molecule can have two distinct electronic configurations in resonance (Figure 8): (I) with a positive charge located at the chromophore group, represented by the N-S conjugate system of the central ring; (II) with a positive charge on one of the auxochrome groups, represented by the terminal amines. Thermodynamic calculations indicate that configuration II is the most abundant at room temperature. Also, mesomer I becomes thermodynamically favorable only at temperatures above 65 °C, while the formation of dimers is thermodynamically favorable for temperatures below 521 °C [41]. Thus, the occurrence of dimers with a resonance structure of mesomer II is expected (Figure 8). The occurrence of tetramers can also be observed, especially at higher concentrations. As expected, the formation of both clusters is unfavorable with increasing temperature, especially for tetramers. However, at temperatures close to room temperature and moderate concentrations (*e.g.*, 20 ppm), a mixture of the different configurations is expected, with a significant proportion of dimers and tetramers [41]. It is noteworthy that the formation of these clusters is responsible for the broadening of the absorption bands and their blue shift, especially in the case of tetramers.

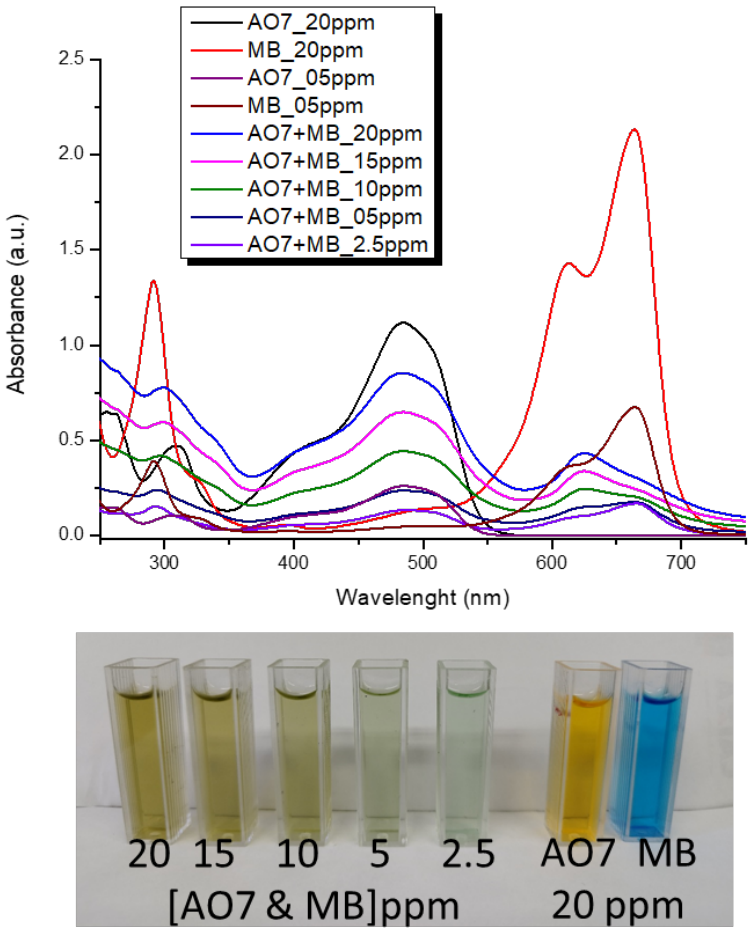


*Figure 7: Absorbance spectra of solutions containing a mixture of equimolar amounts of AO7 and MB at different concentrations. For the sake of comparison, solutions containing only AO7 or MB were also included.*

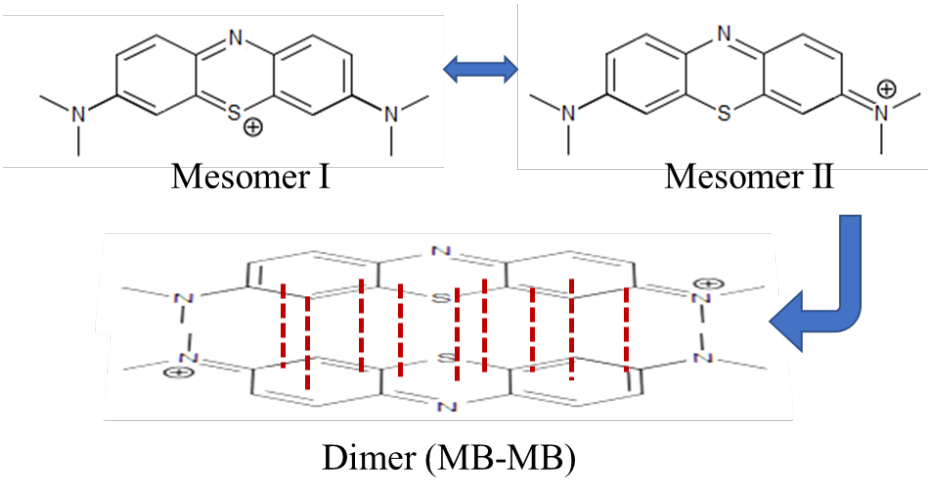


*Figure 8: Possible electronic configuration of the cationic MB molecule and formation of dimers.*

As for the effect observed in the adsorption tests shown in Figure 7, the presence of AO7 may have promoted the formation of MB/AO7 hybrid clusters through electrostatic and π-π interactions between benzene groups, resulting in the formation of organic agglomerates similar to the MB dimers and tetramers described previously. The shape of the spectrum between 550-700 nm for the mixture (AO7&MB)_20ppm is consistent with this assumption. Besides, a decreased intensity of this band was observed. As the concentration of both pollutants decreases, the absorbance spectrum in this spectral region becomes closer to that of MB monomer, with the main peak around 664 nm, although still of lower intensity. The typical region corresponding to that of AO7 (maximum at 484 nm) has a behavior closer to the ideal, indicating that the azo chromophore group of AO7 (R−N=N−R′) plays little role in the formation of the dye agglomerates.

Due to the difficulty in correlating the influence of the concentration of different pollutants with the measured absorbance, several absorbance spectra of mixtures with different concentrations of AO7 and MB between 0 and 20 ppm were obtained and used as a reference (Fig. S4 in Supplementary Material). Figure 9 shows photographs of the aliquots taken during the adsorption tests for the different samples, using a mixture of AO7 and MB. Such tests were carried out with the samples that showed the best performances in the removal of AO7 and MB contaminants in the previous section (single solutions). See Supplementary Material (Section S5) for the absorbance spectra obtained in these tests. By comparing the absorbance spectrum obtained with those with known concentrations of AO7 and MB, an interpolation was performed to calculate the approximate concentrations and the removal efficiency of each sample. The values thus calculated are summarized in Figure 10.

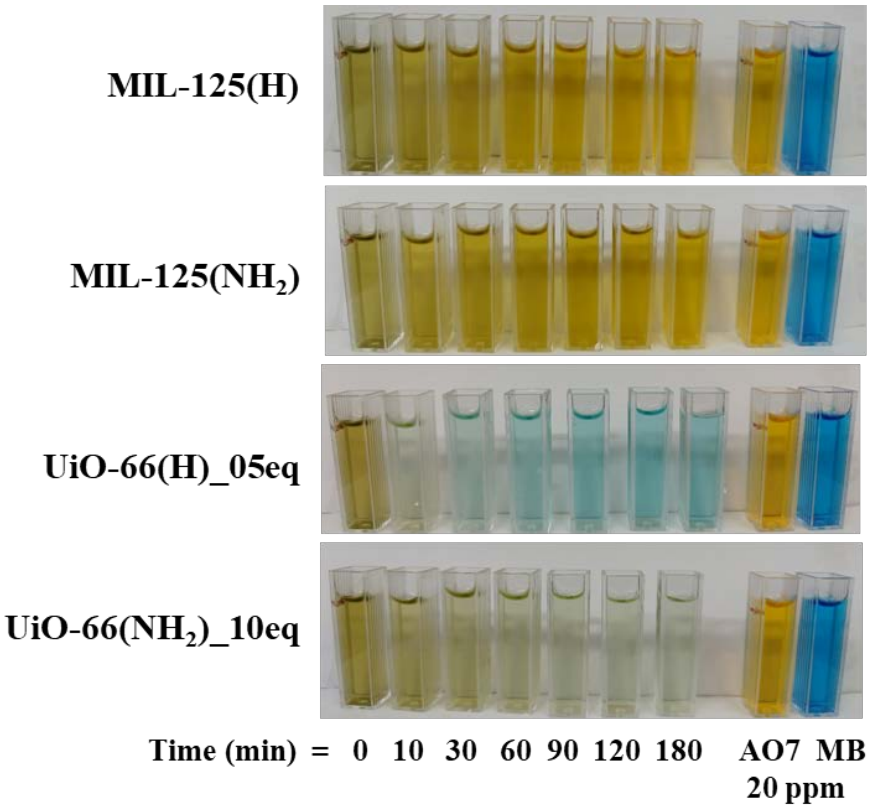


*Figure 9: Image of aliquots taken at different time intervals for each adsorption test performed using a mixture of AO7 and MB at a concentration of 20 ppm each. For the MIL samples, 50 mg.L$^{-1}$ was used, whereas 100 mg.L$^{-1}$ was used for the UiO samples.*

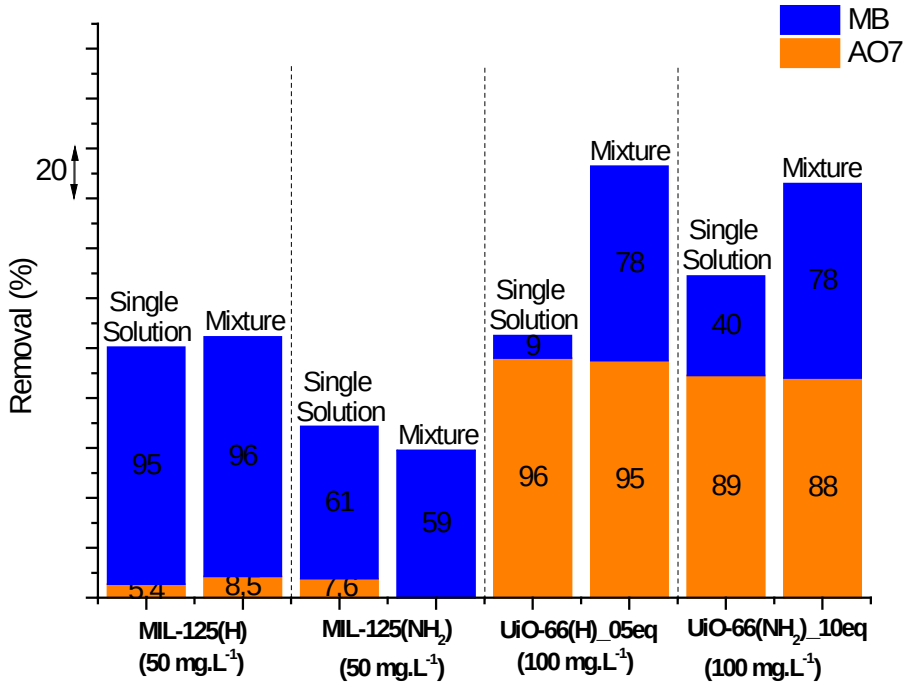


*Figure 10: Comparison of the removal efficiency of AO7 and MB pollutants using different samples and under different conditions. "Single solution" corresponds to the removal capabilities using separate solutions of either AO7 or MB. "Mixture" corresponds to the removal capabilities using the solution resulting from mixing 20 ppm AO7 with 20 ppm MB, labeled as (AO7&MB)_20ppm.*

As observed in the previous section, the MIL family showed much higher adsorption efficiencies for the cationic MB and the UiO family for the anionic AO7. In both cases, unmodified versions of each material performed better than their aminated counterparts. In solution with a mixture of these contaminants, both maintained similar removal efficiencies to those previously observed (single solution vs. mixture – Figure 10), considering the contaminant with the highest affinity (AO7 for UiO and MB for MIL). Thus, it can be concluded that the presence of a second oppositely charged contaminant has little effect on the adsorption mechanism of the species with greater affinity for the adsorbent in question. Regarding the pollutant with lower affinity, some differences were observed when the solution contained the (AO7&MB)_20ppm mixture. While the MIL-125 family continued to reject virtually all of the anionic AO7, the UiO-66 family showed

a significant increase in adsorption of the cationic MB. This behavior indicates a fundamental difference in the adsorption mechanism of the two MOFs studied here. As also discussed in our previous work [17], the adsorption of AO7 on UiO-66 is mainly governed by electrostatic interactions between the sulfonic group ($-SO_3^-$) present in the AO7 molecule and the inorganic core $Zr_6O_4(OH)_4$ of UiO-66. It has been shown that such interaction is favored in defective UiO-66 frameworks (especially in the form of missing linkers) due to the easier accessibility of pollutant molecules to the inorganic clusters [17]. This behavior leaves the rest of the molecule, dominated by benzene groups, free to interact with other organic molecules such as MB through hydrophobic and π-π interactions. Thus, the previously existing AO7/MB agglomerates can be maintained and adsorbed onto UiO-66 through these sulfonic groups. On the other hand, the adsorption of MB on MIL-125 is governed by the interaction with the organic linker (BDC) through electrostatic and π-π interactions [18]. For this reason, the AO7/MB organic clusters previously formed in the solution may be disrupted by the addition of the adsorbent, since such molecules are linked by interactions of the same type. The obtained results suggest that the interaction between MB and BDC is thermodynamically more favorable than the interaction between MB and AO7. This is because there was no significant change in the adsorption capacity of MIL-125 when the pollutants were found mixed in solution. Therefore, it can be concluded that the actual selectivity of the UiO-66 family is much lower than what would be the ideal selectivity due to the coadsorption of the cationic MB previously bound to AO7. The actual selectivity of the MIL-125 family is very close to ideal because the previously formed AO7/MB agglomerates are broken apart when the MB begins to interact with the adsorption sites present in the MIL-125 structure.

### 3.4. Stability tests in aqueous solution

The best-performing samples in each series were subjected to two stability tests. The first test consisted of suspending the samples in water for 24 h and drying directly at 100 ˚C overnight. The second test consisted of performing adsorption tests of either MB or AO7 and washing the samples with EtOH before drying at 100 ˚C overnight. UiO-66 showed excellent stability in water, even when dried from the water suspension at 100 °C (Figure 11a), for the both non-functionalized and functionalized (-$NH_2$) versions. MIL-125, on the other hand, showed much less stability (Figure 11b). The non-aminated version, MIL-125(H), experienced a complete collapse of its crystalline framework. In this case, the formation of different crystalline structures is evident, consisting of a mixture of crystalline terephthalic acid, nanocrystalline $TiO_2$, and possibly an amorphous phase. It is believed that the structural collapse of MIL-125(H) begins immediately after its addition to water, which is accompanied by audible crepitation. The greater stability of UiO-66 compared to MIL-125 was also confirmed by FTIR (Figs. S9 and S10 – Supplementary Material) [35,43,44]. It can be seen that the greater stability of UiO-66 can be explained by the fact that Ti has a higher electronegativity than Zr, in addition to having a lower coordination number (CN) with neighboring O species (CN = 6 vs. 8 for Zr). Thus, nucleophilic species are more likely to attack the metallic cores of MIL-125, even though such cores have the same coordination number with the organic ligands as in UiO-66 (CN = 12). This reasoning finds support in the reactivity of alkoxides involving tetravalent metals such as Ti and Zr [45]. Furthermore, the more open structure of the SBU corresponding to MIL-125 certainly contributes to easier access to reactive species. The aminated version, MIL-125($NH_2$), on the other hand, appears to retain its crystalline structure, as well as the other structures of the UiO-66 family, as also confirmed by FTIR.

This difference in water stability between the aminated and non-aminated versions of MIL-125, as well as other MOFs, has been similarly reported elsewhere [15,16]. It has been reported that the greater stability of structures with an amino group is due to an intramolecular interaction via hydrogen bonding between the H of the amino group and the O of the carboxylate attached to the inorganic cluster. The adsorption process in both the UiO-66 and MIL-125 families seems to have little influence on the structural stability of the MOFs, and the small variations observed, especially concerning the MIL series, are mainly due to the instability in water and not to the adsorption process itself. By comparison, the drying process from aqueous suspension at 100 $^{\circ}$C seems to be much more detrimental to the stability of MIL-125(H), which may be related to an increased kinetics of structural collapse due to the chemical attack of water molecules.

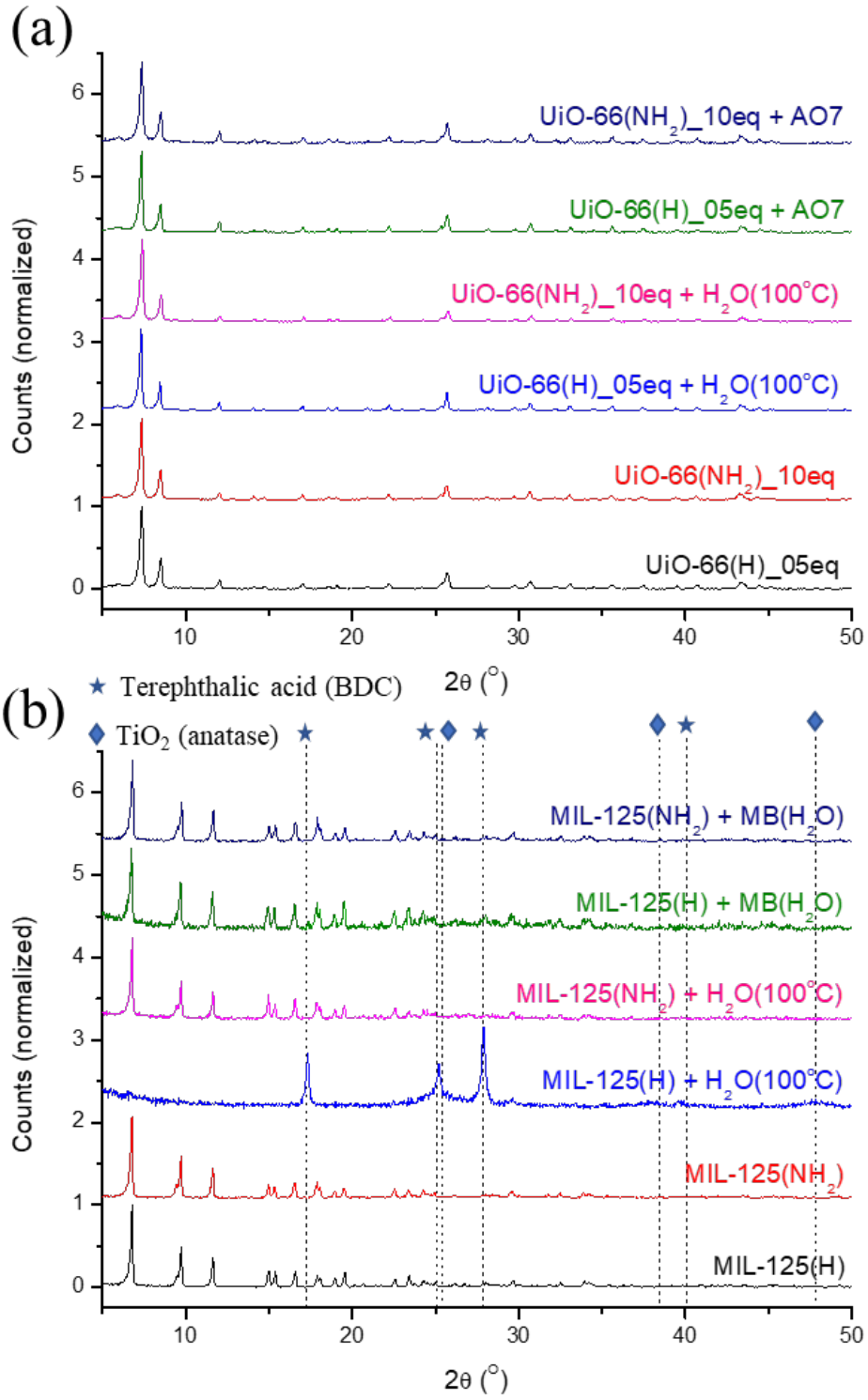


*Figure 11: Stability tests of the different MOFs in water for 24 h (air-drying at 100 °C) and after adsorption of MB or AO7 (washed with EtOH before drying).*

## 4. Conclusions

In this work, it was possible to compare different MOF structures in terms of their textural, surface, and adsorption properties. The size and morphology of both aminated and non-aminated UiO-66 crystals, as well as their pore structure, could be finely tuned by the addition of water to the reaction medium, allowing control over the level of defects in the structure. As a result, their adsorption performance could be effectively improved, with a maximum adsorption capacity when moderate molar fractions ($H_2O$/Zr) of water were added. UiO-66(H)_5eq and UiO-66($NH_2$)_10eq showed the highest adsorption performance for the unfunctionalized and amino-functionalized groups, respectively. Specifically, UiO-66(H)_5eq showed superior performance over UiO-66($NH_2$)_10eq in the adsorption of the anionic dye AO7, removing 96% of the contaminant after 180 min compared to only 89% for the latter. This improvement is due to the synergy of several features, in particular the increase in SSA and the expansion of the microporous structure, coupled with the maintenance of an appropriate surface charge. Together, these factors allow for improved interaction with the target pollutant. While the UiO-66 samples showed a higher affinity for anionic species (AO7), the opposite was observed for the MIL-125 frameworks, which practically adsorbed only cationic species (MB). Such adsorption properties can be explained in terms of surface charge and electrostatic interaction, with MIL-125 materials typically displaying more negative PZC compared to UiO-66. Within the MIL-like samples, the non-functionalized MIL-125(H) showed significantly superior adsorption of MB. This observation contrasts with some previous studies suggesting a higher efficiency of MIL-125($NH_2$) due to specific interactions with the amino group. In this work, the reduced performance of the aminated version could be attributed to a significantly smaller SSA and pore size, leading to a reduction in the

number and accessibility of adsorption sites. The adsorption mechanism of the different dyes was found to be fundamentally different: the anionic AO7 coordinates more specifically with the inorganic clusters, whereas the cationic MB interacts in a more delocalized manner with the organic linkers. Such adsorption mechanisms could be observed experimentally when a mixture of AO7 and MB was used in the adsorption tests. The previously formed AO7/MB agglomerates are maintained when UiO-66 materials are used as adsorbents since the interaction mechanisms are fundamentally different and do not interfere with each other. However, when the MIL-125 materials are used, the previously formed AO7/MB agglomerates break apart because the interaction mechanisms are fundamentally similar, and a higher affinity between the MOF and MB is observed. Finally, the materials were tested for stability. The high instability of MIL-125(H) in water was evident, while the other structures UiO-66(H), UiO-66($NH_2$), and MIL-125($NH_2$) showed high stability, even when dried from water suspension at 100°C. In MIL-125, the amino group is probably responsible for the higher framework stability, which can be explained by intramolecular hydrogen bonding.

## Acknowledgments

This work was supported by FAPEMIG (APQ-00792-17), CNPq (306193/2020-5, 403191/2021-1, and 304415/2021-9) and CAPES (PROEX / 001). The authors are grateful for the technical support from Centro de Microscopia/UFMG and CTNano

## References

[1] I. Ihsanullah, Applications of MOFs as adsorbents in water purification: Progress, challenges and outlook, Curr. Opin. Environ. Sci. Heal. 26 (2022) 100335. https://doi.org/10.1016/j.coesh.2022.100335.

[2] P.O. Oladoye, S.A. Adegboyega, A.R.A. Giwa, Remediation potentials of composite metal-organic frameworks (MOFs) for dyes as water contaminants: A comprehensive review of recent literatures, Environ. Nanotechnology, Monit. Manag. 16 (2021) 100568. https://doi.org/10.1016/j.enmm.2021.100568.

[3] P.H.M. Andrade, N. Henry, C. Volkringer, T. Loiseau, H. Vezin, M. Hureau, A. Moissette, Iodine Uptake by Zr-/Hf-Based UiO-66 Materials: The Influence of Metal Substitution on Iodine Evolution, ACS Appl. Mater. Interfaces. 14 (2022) 29916–29933. https://doi.org/10.1021/acsami.2c07288.

[4] H.C. Zhou, J.R. Long, O.M. Yaghi, Introduction to metal-organic frameworks, Chem. Rev. 112 (2012) 673–674. https://doi.org/10.1021/cr300014x.

[5] Y. Cao, X. Chen, X. Li, B. Wang, Tuning Surface Functionalization and Pore Structure of UiO-66 Metal–Organic Framework Nanoparticles for Organic Pollutant Elimination, ACS Appl. Nano Mater. 4 (2021) 5486–5495. https://doi.org/10.1021/ACSANM.1C00796.

[6] O.K. Farha, I. Eryazici, N.C. Jeong, B.G. Hauser, C.E. Wilmer, A.A. Sarjeant, R.Q. Snurr, S.T. Nguyen, A.Ö. Yazaydın, J.T. Hupp, Metal–Organic Framework Materials with Ultrahigh Surface Areas: Is the Sky the Limit?, J. Am. Chem. Soc. 134 (2012) 15016–15021. https://doi.org/10.1021/ja3055639.

[7] V. Guillerm, F. Ragon, M. Dan-Hardi, T. Devic, M. Vishnuvarthan, B. Campo, A. Vimont, G. Clet, Q. Yang, G. Maurin, G. Férey, A. Vittadini, S. Gross, C. Serre, A series of isoreticular, highly stable, porous zirconium oxide based metal-organic

frameworks, Angew. Chemie - Int. Ed. 51 (2012) 9267–9271. https://doi.org/10.1002/anie.201204806.

[8] S. Dhaka, R. Kumar, A. Deep, M.B. Kurade, S.W. Ji, B.H. Jeon, Metal–organic frameworks (MOFs) for the removal of emerging contaminants from aquatic environments, Coord. Chem. Rev. 380 (2019) 330–352. https://doi.org/10.1016/j.ccr.2018.10.003.

[9] T. Devic, C. Serre, High valence 3p and transition metal based MOFs, Chem. Soc. Rev. 43 (2014) 6097–6115. https://doi.org/10.1039/C4CS00081A.

[10] S. Yuan, L. Feng, K. Wang, J. Pang, M. Bosch, C. Lollar, Y. Sun, J. Qin, X. Yang, P. Zhang, Q. Wang, L. Zou, Y. Zhang, L. Zhang, Y. Fang, J. Li, H.-C. Zhou, Stable Metal-Organic Frameworks: Design, Synthesis, and Applications, Adv. Mater. 30 (2018) 1704303. https://doi.org/10.1002/adma.201704303.

[11] L. Wang, X. Li, B. Yang, K. Xiao, H. Duan, H. Zhao, The chemical stability of metal-organic frameworks in water treatments: Fundamentals, effect of water matrix and judging methods, Chem. Eng. J. 450 (2022) 138215. https://doi.org/10.1016/j.cej.2022.138215.

[12] Z. Yu, X. Cao, S. Wang, H. Cui, C. Li, G. Zhu, Research Progress on the Water Stability of a Metal-Organic Framework in Advanced Oxidation Processes, Water. Air. Soil Pollut. 232 (2021). https://doi.org/10.1007/s11270-020-04953-9.

[13] S.-Y. Fang, P. Zhang, J.-L. Gong, L. Tang, G.-M. Zeng, B. Song, W.-C. Cao, J. Li, J. Ye, Construction of highly water-stable metal-organic framework UiO-66 thin-film composite membrane for dyes and antibiotics separation, Chem. Eng. J. 385 (2020) 123400. https://doi.org/10.1016/j.cej.2019.123400.

[14] J.H. Cavka, S. Jakobsen, U. Olsbye, N. Guillou, C. Lamberti, S. Bordiga, K.P. Lillerud, A New Zirconium Inorganic Building Brick Forming Metal Organic

Frameworks with Exceptional Stability, J. Am. Chem. Soc. 130 (2008) 13850–13851. https://doi.org/10.1021/ja8057953.

[15] A.S.Y. Liew, S.E. Teo, S.Y. Nguang, N.S. Rizalman, N. Tahir, S.R. Wong, P.Y. Moh, Feasibility of NH2-MIL-125 as an Adsorbent for the Removal of Organic Pollutant in Water, Trans. Sci. Technol. 7 (2020) 198–203.

[16] S.N. Kim, J. Kim, H.Y. Kim, H.Y. Cho, W.S. Ahn, Adsorption/catalytic properties of MIL-125 and NH2-MIL-125, Catal. Today. 204 (2013) 85–93. https://doi.org/10.1016/j.cattod.2012.08.014.

[17] H.G. Palhares, A.G. Leonel, R.L. Oréfice, R.O. Correia, D. Riassetto, M. Langlet, M. Houmard, E.H.M. Nunes, Tailoring the pore architecture and crystalline structure of UiO-66 for the selective adsorption of anionic species in aqueous media, Environ. Nanotechnology, Monit. Manag. 20 (2023) 100869. https://doi.org/10.1016/j.enmm.2023.100869.

[18] Y.H. Fan, S.W. Zhang, S. Bin Qin, X.S. Li, S.H. Qi, An enhanced adsorption of organic dyes onto NH2 functionalization titanium-based metal-organic frameworks and the mechanism investigation, Microporous Mesoporous Mater. 263 (2018) 120–127. https://doi.org/10.1016/j.micromeso.2017.12.016.

[19] P.H.M. Andrade, H. Ahouari, C. Volkringer, T. Loiseau, H. Vezin, M. Hureau, A. Moissette, Electron-Donor Functional Groups, Band Gap Tailoring, and Efficient Charge Separation: Three Keys To Improve the Gaseous Iodine Uptake in MOF Materials, ACS Appl. Mater. Interfaces. 15 (2023) 31032–31048. https://doi.org/10.1021/acsami.3c04955.

[20] F. Ambroz, T.J. Macdonald, V. Martis, I.P. Parkin, Evaluation of the BET theory for the characterization of meso and microporous MOFs, Small Methods. 2 (2018) 1800173. https://doi.org/10.1002/smtd.201800173.

[21] J. Li, J.L. Gong, G.M. Zeng, P. Zhang, B. Song, W.C. Cao, H.Y. Liu, S.Y. Huan, Zirconium-based metal organic frameworks loaded on polyurethane foam membrane for simultaneous removal of dyes with different charges, J. Colloid Interface Sci. 527 (2018) 267–279. https://doi.org/10.1016/J.JCIS.2018.05.028.

[22] H. Guo, F. Lin, J. Chen, F. Li, W. Weng, Metal-organic framework MIL-125(Ti) for efficient adsorptive removal of Rhodamine B from aqueous solution, Appl. Organomet. Chem. 29 (2015) 12–19. https://doi.org/10.1002/aoc.3237.

[23] J. Qiu, Y. Feng, X. Zhang, M. Jia, J. Yao, Acid-promoted synthesis of UiO-66 for highly selective adsorption of anionic dyes: Adsorption performance and mechanisms, J. Colloid Interface Sci. 499 (2017) 151–158. https://doi.org/10.1016/J.JCIS.2017.03.101.

[24] S. Lin, Y. Zhao, Y.-S. Yun, Highly Effective Removal of Nonsteroidal Anti-inflammatory Pharmaceuticals from Water by Zr(IV)-Based Metal–Organic Framework: Adsorption Performance and Mechanisms, ACS Appl. Mater. Interfaces. 10 (2018) 28076–28085. https://doi.org/10.1021/ACSAMI.8B08596.

[25] X.M. Cheng, X.Y. Dao, S.Q. Wang, J. Zhao, W.Y. Sun, Enhanced Photocatalytic CO2 Reduction Activity over NH2-MIL-125(Ti) by Facet Regulation, ACS Catal. 11 (2021) 650–658. https://doi.org/10.1021/acscatal.0c04426.

[26] V. V. Butova, K.S. Vetlitsyna-Novikova, I.A. Pankin, K.M. Charykov, A.L. Trigub, A. V. Soldatov, Microwave synthesis and phase transition in UiO-66/MIL-140A system, Microporous Mesoporous Mater. 296 (2020) 109998. https://doi.org/10.1016/J.MICROMESO.2020.109998.

[27] Z. Li, G. Che, W. Jiang, L. Liu, H. Wang, Visible-light-driven CQDs@MIL-125(Ti) nanocomposite photocatalyst with enhanced photocatalytic activity for the degradation of tetracycline, RSC Adv. 9 (2019) 33238–33245.

https://doi.org/10.1039/c9ra05600a.

[28] M. Dan-Hardi, C. Serre, T. Frot, L. Rozes, G. Maurin, C. Sanchez, G. Férey, A New Photoactive Crystalline Highly Porous Titanium(IV) Dicarboxylate, J. Am. Chem. Soc. 131 (2009) 10857–10859. https://doi.org/10.1021/ja903726m.

[29] X. Liu, Metal-organic framework UiO-66 membranes, Front. Chem. Sci. Eng. 14 (2020) 216–232. https://doi.org/10.1007/s11705-019-1857-5.

[30] O.K. Farha, J.T. Hupp, Rational Design, Synthesis, Purification, and Activation of Metal−Organic Framework Materials, Acc. Chem. Res. 43 (2010) 1166–1175. https://doi.org/10.1021/ar1000617.

[31] O.K. Farha, C.D. Malliakas, M.G. Kanatzidis, J.T. Hupp, Control over catenation in metal-organic frameworks via rational design of the organic building block, J. Am. Chem. Soc. 132 (2010) 950–952. https://doi.org/10.1021/ja909519e.

[32] M.J. Katz, Z.J. Brown, Y.J. Colón, P.W. Siu, K.A. Scheidt, R.Q. Snurr, J.T. Hupp, O.K. Farha, A facile synthesis of UiO-66, UiO-67 and their derivatives, Chem. Commun. 49 (2013) 9449. https://doi.org/10.1039/c3cc46105j.

[33] G.C. Shearer, S. Chavan, J. Ethiraj, J.G. Vitillo, S. Svelle, U. Olsbye, C. Lamberti, S. Bordiga, K.P. Lillerud, Tuned to Perfection: Ironing Out the Defects in Metal–Organic Framework UiO-66, Chem. Mater. 26 (2014) 4068–4071. https://doi.org/10.1021/cm501859p.

[34] A.H. Ibrahim, W.A. El-Mehalmey, R.R. Haikal, M.E.A. Safy, M. Amin, H.R. Shatla, S.G. Karakalos, M.H. Alkordi, Tuning the Chemical Environment within the UiO-66-NH2 Nanocages for Charge-Dependent Contaminant Uptake and Selectivity, Inorg. Chem. 58 (2019) 15078–15087. https://doi.org/10.1021/acs.inorgchem.9b01611.

[35] C. Nanthamathee, C. Chantarangkul, C. Jakkrawhad, A. Payaka, P.

Dechatiwongse, Fine-tuning the dye adsorption capacity of UiO-66 by a mixed-ligand approach, Heliyon. 8 (2022). https://doi.org/10.1016/J.HELIYON.2022.E08961.

[36] A. Zhang, B. Liu, M. Liu, Z. Xie, D. Wang, G. Feng, The adsorption properties of defect controlled metal-organic frameworks of UiO-66, Sep. Purif. Technol. 270 (2021) 118842. https://doi.org/10.1016/j.seppur.2021.118842.

[37] M. Aghajanzadeh, M. Zamani, H. Molavi, H. Khieri Manjili, H. Danafar, A. Shojaei, Preparation of Metal–Organic Frameworks UiO-66 for Adsorptive Removal of Methotrexate from Aqueous Solution, J. Inorg. Organomet. Polym. Mater. 28 (2018) 177–186. https://doi.org/10.1007/s10904-017-0709-3.

[38] Y. Cao, H. Zhang, F. Song, T. Huang, J. Ji, Q. Zhong, W. Chu, Q. Xu, UiO-66-NH2/GO composite: Synthesis, characterization and CO2 adsorption performance, Materials (Basel). 11 (2018). https://doi.org/10.3390/ma11040589.

[39] J. Zhang, Y. Hu, J. Qin, Z. Yang, M. Fu, TiO2-UiO-66-NH2 nanocomposites as efficient photocatalysts for the oxidation of VOCs, Chem. Eng. J. 385 (2020) 123814. https://doi.org/10.1016/j.cej.2019.123814.

[40] M. Alfè, V. Gargiulo, M. Amati, V.A. Maraloiu, P. Maddalena, S. Lettieri, Mesoporous tio2 from metal-organic frameworks for photo-luminescence-based optical sensing of oxygen, Catalysts. 11 (2021). https://doi.org/10.3390/catal11070795.

[41] A. Fernandez-Perez, G. Marban, Visible light spectroscopic analysis of methylene blue in water; what comes after dimer?, ACS Omega. 5 (2020) 29801–29815. https://doi.org/10.1021/acsomega.0c03830.

[42] I. Khan, K. Saeed, I. Zekker, B. Zhang, A.H. Hendi, A. Ahmad, S. Ahmad, N. Zada, H. Ahmad, L.A. Shah, T. Shah, I. Khan, Review on Methylene Blue: Its

Properties, Uses, Toxicity and Photodegradation, Water (Switzerland). 14 (2022). https://doi.org/10.3390/w14020242.

[43] P.H.M. Andrade, N. Henry, C. Volkringer, T. Loiseau, H. Vezin, M. Hureau, A. Moissette, Iodine Uptake by Zr-/Hf-Based UiO-66 Materials: The Influence of Metal Substitution on Iodine Evolution, ACS Appl. Mater. Interfaces. (2022). https://doi.org/10.1021/acsami.2c07288.

[44] S.M.F. Vilela, P. Salcedo-Abraira, L. Micheron, E.L. Solla, P.G. Yot, P. Horcajada, A robust monolithic metal-organic framework with hierarchical porosity, Chem. Commun. 54 (2018) 13088–13091. https://doi.org/10.1039/c8cc07252c.

[45] J. Blanchard, M. In, B. Schaudel, C. Sanchez, Hydrolysis and Condensation Reactions of Transition Metal Alkoxides: Calorimetric Study and Evaluation of the Extent of Reaction, Eur. J. Inorg. Chem. 1998 (1998) 1115–1127. https://doi.org/10.1002/(SICI)1099-0682(199808)1998:8<1115::AID-EJIC1115>3.0.CO;2-N.